

Electrochemical Behavior and Properties of Passive Films on 304 Stainless Steel under High Temperature and Stress Conditions

Shanlin He^{1,*}, Daming Jiang¹

School of Materials Science and Engineering, Harbin Institute of Technology, Harbin 150001, China

*E-mail: 11B909025@hit.edu.cn

Received: 27 January 2018 / Accepted: 22 March 2018 / Published: 10 May 2018

Polarization curves, electrochemical impedance spectroscopy (EIS), X-ray photoelectron spectroscopy (XPS), atomic force microscopy (AFM) and scanning electron microscopy (SEM) were used to investigate the evolution of the electrochemical behavior and the properties of passive films on 304 stainless steel under high temperature and high stress conditions. The results showed that the proportion of each phase in the film considerably changed as the immersion time increased but eventually approached a stable value. The change in the film resistance R_m was mainly affected by the intergranular corrosion the surface. A correlation of the evolution of the electrochemical behavior with the phase contents in the passive film and surface morphology was investigated.

Keywords: metals and alloys; thin films; composition fluctuations; corrosion; grain boundaries

1. INTRODUCTION

304 stainless steel exhibits excellent corrosion resistance and has been widely used in the nuclear power, construction, and chemical industries [1-8]. Despite the excellent corrosion resistance, stainless steel can also undergo stress corrosion cracking due to the effects of temperature, media, and stress in the work environment, which all cause damage. The corrosion resistance of stainless steel is closely related to the properties of its surface passive film [9,10]. The composition and structural properties of surface passive films formed on 304 stainless steel have been extensively studied [11-14]. The passive film possesses a duplex-layer structure consisting of an internal oxide layer and an external hydroxide layer, and the main chemical components are $\text{Cr}^{3+}(\text{ox})$, $\text{Fe}^{3+}(\text{ox})$, $\text{Fe}^{2+}(\text{ox})$, $\text{Fe}(\text{OH})_3$, and $\text{Cr}^{3+}(\text{hyd})$ [15]. In a high temperature water environment, the electrochemical properties of the oxide film will change with changing immersion environment [15-26]. The protective properties of passive films are compromised as the temperature increases [21]. In a high temperature water

environment, the corrosion resistance of the passive film is enhanced by increasing the immersion time, and the corrosion rate is primarily determined by the inner chromium-rich layer [27]. The oxide content and the film thickness will change as the temperature changes [15]. The pre-formed oxide layer of hematite on the substrate surface varies as the environment changes, and it becomes loose and porous with the dissolution of Cr [24]. When the concentration of dissolved oxygen decreases, the amount of hematite on the surface drops to form spinel oxides [28]. Researchers have also explored the effects of dissolved oxygen concentration on the chemical composition and density of the oxide layer, and they proposed theoretical models to characterize the electrochemical properties of the corrosion process [17,25,29]. In an immersion environment, stress can increase the adsorbed oxygen level on the surface of a passive film and even rupture the passive film, thereby exposing the metal substrate to the solution [30]. Bojinov [25] and Kuang [28] found that the diffusion coefficients of films immersed for different times (1 and 3 days) can differ by several orders of magnitude. Therefore, a longer period of monitoring is required to understand the changes in the corrosion resistance of materials during service.

The conclusions of the abovementioned research are drawn in a stress free immersion environments [15-20]. However, under working conditions, the material surfaces usually experience stress and deformation that are considerably greater than the internal stress due to various types of load. The deformation stress can even reach the yield stress of the material, which results in film rupture and acceleration of substrate corrosion [30]. However, in a high temperature water environment, only a few studies have been reported on the mechanism of corrosion resistance of 304 stainless steel under high stress. Although researchers have studied the evolution of electrochemical properties of films on 304 stainless steel with immersion time [18,24], the surface morphology was not included in their analysis. Based on the previous studies, the corrosion behavior of passive films formed on the surface of 304 stainless steel cannot be accurately predicted under the above conditions [28].

The passive film is the critical factor to ensure the corrosion resistance of materials, and conducting an in-depth study of the evolution of its performance is necessary. The focus of this study is the corrosion behavior of 304 stainless steel under a high-temperature water environment and high stress conditions. The methods of X-ray photoelectron spectroscopy (XPS), atomic force microscopy (AFM), electrochemical impedance spectroscopy (EIS) and potentiodynamic polarization curve were employed to analyze the changes in the chemical composition and surface morphology of passive films and the electrochemical performance of the material. This study discussed the relationship between the evolution of the electrochemical behavior and changes in the properties of passive films in detail, and the research conclusions were validated by the long-term immersion test.

2. EXPERIMENTAL

Cold-rolled 304 austenitic stainless steel plates with thickness of 1mm were used in this study. The samples were heat treated to 1050 °C and kept for 30 minutes, and then cooled to room temperature in air. The chemical composition is shown in Table 1.

Table 1. Chemical composition of 304 stainless steel (wt.%).

| C | N | Si | Mn | S | P | Cu | Co | B | Ni | Cr | Fe |
|--------|--------|--------|-------|--------|--------|-------|-------|---------|------------|------------|------|
| ≤0.035 | ≤0.080 | ≤0.54% | ≤1.27 | ≤0.015 | ≤0.030 | ≤1.00 | ≤0.06 | ≤0.0019 | ≤9.00-1.00 | ≤18.5-20.0 | Bal. |

For the formation of passive film, the samples were polished by SiC sandpaper and immersed in acid pickling solution with composition of 20% nitric acid, 5% hydrofluoric acid and 75% water, then washed in deionized water. Immersion tests under constant load were carried out in 90 °C deionized water through employing the way of beam, the samples were cut into uniform strength section as shown in Fig. 1. There were constant stresses with value of 100 MPa which uniformly distributed on the surfaces of the samples during the loading process, and the fixture was made of the same material as the sample to avoid the influence of the galvanic corrosion.

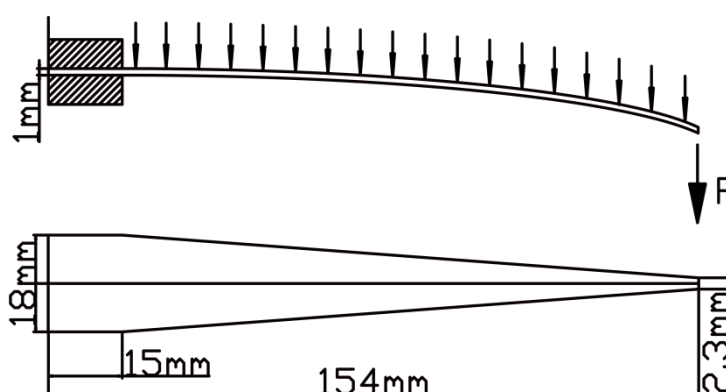


Figure 1. Dimension and loading form of the sample under constant load(uniform strength section).

After the immersion test, the potentiodynamic polarization curve and electrochemical impedance spectroscopy (EIS) were carried out in the same condition as the immersion test through employing Gamry Reference 3000 electrochemical system. Three electrodes system were used for the test, the reference electrode was a silver chloride electrode, the working electrode was the sample and the graphite was used as the counter electrode. For the potentiodynamic polarization curve, the potential scanning speed was 0.5 mV s⁻¹. For the EIS measurement, a sinusoidal signal with amplitude of 10 mV was applied on the samples based on the open circuit potential and the testing frequency ranged from 100000 Hz to 0.01 Hz for data collection, the EIS data was fitted through ZSimpWin software.

The samples after immersion tests were cut into small pieces with testing area of 1.6 mm² (0.8 mm × 2 mm) for the X-ray photoelectron spectroscopy (XPS) analyses which were carried out through employing PHI 5700 ESCA System spectrometer. The X-ray source was Al-Kα (1486.6 eV) without monochromator and the spectrometer was used with constant pass energy of 187.85 eV (wide scan) and 23.5 eV (narrow scan). The XPS data was analyzed through XPS Peak Fit 4.1 software. The average thickness of the passive film was calculated from the equations shown as follow[15]:

$$\frac{I_{Fe}^{met}}{I_{Fe}^0} = \left\{ \exp\left(-\frac{t_{pass}}{\lambda_{Fe}^{pass}}\right) \right\} \cdot \left\{ \exp\left(-\frac{t_{cont}}{\lambda_{Fe}^{cont}}\right) \right\} \tag{1}$$

$$\frac{I_c^{cont}}{I_c^{graphite}} = \frac{\lambda_C^{cont}}{\lambda_C^{graphite}} \cdot \frac{C_C^{cont}}{C_C^{graphite}} \cdot \left\{ 1 - \exp\left(-\frac{t_{cont}}{\lambda_C^{cont}}\right) \right\} \tag{2}$$

where I_{Fe}^{met} and I_{Fe}^0 were the photoelectron intensity of the underlying steel and the Fe metal without passive film, respectively. t_{pass} was the average thickness of passive film. λ_{Fe}^{pass} and λ_{Fe}^{cont} were the inelastic mean free path of photoelectron from the Fe metal which passed through the passive film and the contaminant hydrocarbon layer, respectively. I_c^{cont} and $I_c^{graphite}$ were the photoelectron intensity of the carbon in the contaminant layer and the pure graphite, respectively. C_c^{cont} and $C_c^{graphite}$ were the atomic concentration of the carbon in the contaminant carbon and the graphite, respectively. The inelastic mean free path for the calculation are displayed in Table 2.

Table 2. Inelastic mean free path of the electron for the caculation of average thickness of the passive film through X-ray photoelectron spectroscopy (XPS) analysis.

| $\lambda_C^{graphite}$ (nm) | λ_C^{cont} (nm) | λ_{Fe}^{cont} (nm) | λ_{Fe}^{met} (nm) | $\lambda_{Fe}^{ox,hyd}$ (nm) |
|-----------------------------|-------------------------|----------------------------|---------------------------|------------------------------|
| 1.77 | 3.04 | 2.43 | 1.39 | 2.50 |

The surface morphology of the samples were observed through using scanning electron microscope (SEM, JEOL, JSM-5800) and atomic force microscope (AFM, Bruker, Dimension Icon).

3. RESULTS AND DISCUSSION

3.1 Electrochemical analysis

Fig. 2 shows the potentiodynamic polarization curves of the samples for different immersion times. As shown, a obvious passivation region could be observed on the polarization curve of the sample before immersion test (0 day). The results indicated that as the immersion time increased, the breakdown potential of the sample gradually decreased, which implied a decreasing corrosion resistance during the immersion process.

Fig. 3(a) displays the electrochemical impedance spectroscopy of the samples for different immersion times, which could be fitted by using the equivalent circuit model shown in Fig. 3(b). There were two time constants in this model, R_s was the resistance of solution, R_m was the resistance of passive film, Q_m was the constant phase element for passive film, C_{dl} was the constant phase element for electrochemical double layer and R_{ct} was the resistance of charge transfer. A good correspondence could be observed between the fitting data (solid lines and solid symbols) and the experimental data (hollow symbols), which implied good accuracy and low error for the fitting results.

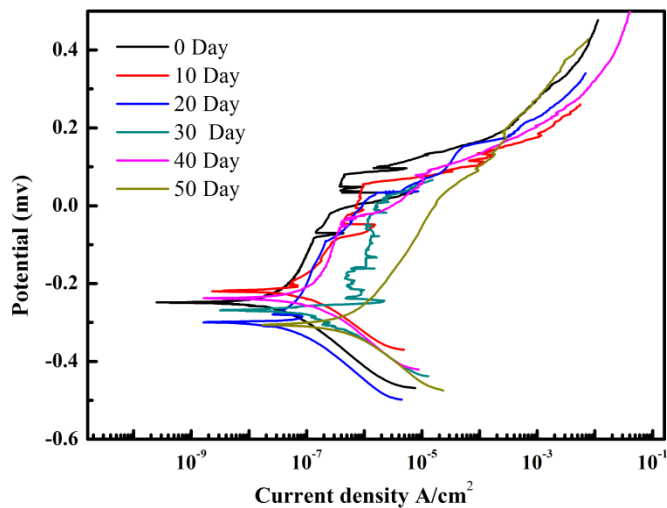


Figure 2. Potentiodynamic polarization curves of the samples under constant stress of 100 MPa for different immersion times in 90 °C deionized water.

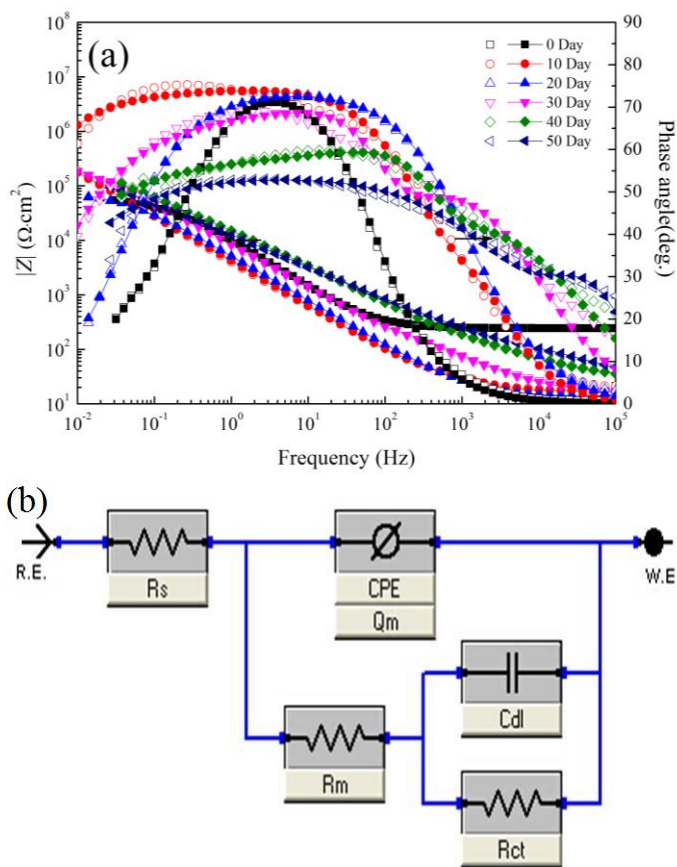


Figure 3. Electrochemical impedance spectroscopy and equivalent circuit model of the samples under constant stress of 100 MPa for different immersion times in 90 °C deionized water: (a) Bode plots; (b) equivalent circuit model.

The fitting resistance of passive film is exhibited in Fig. 4. The results showed that the resistance of passive film decreased with the increase of immersion time, which changed from 700 Ω before the immersion test to 75 Ω after immersion for 20 days. The resistance became to 25 Ω after immersion for 30 days and then tended to be stable. The decreasing resistance suggested the reduction of resistance for the ions passing through the passive film. The obvious decline of resistance indicated that the corrosion resistance of passive film had significantly changed during the immersion process.

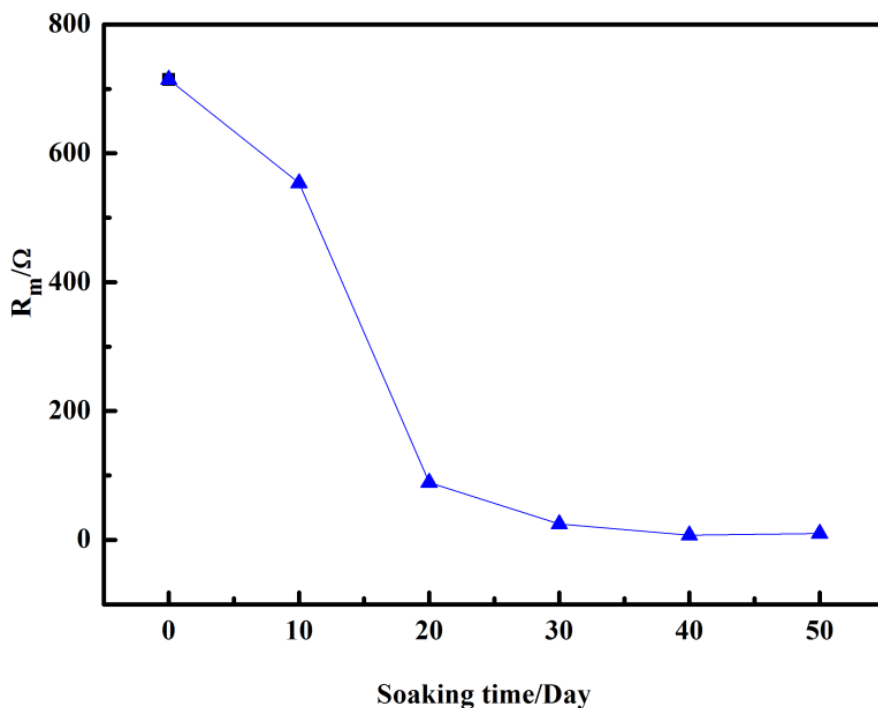
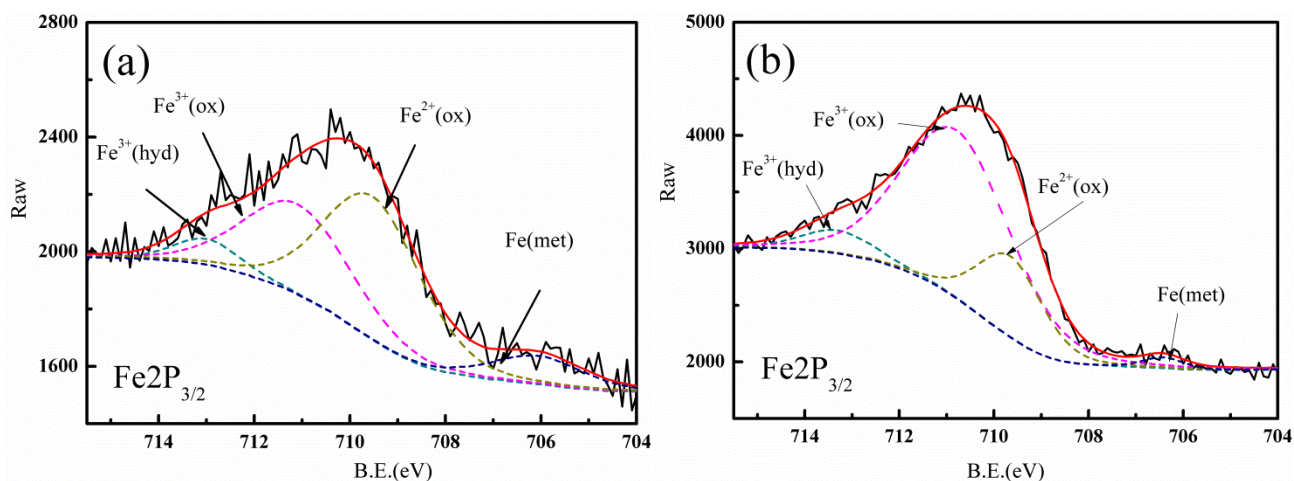


Figure 4. Variation of passive film resistance with immersion times under constant stress of 100 MPa in 90 °C deionized water.

3.1. XPS analyses



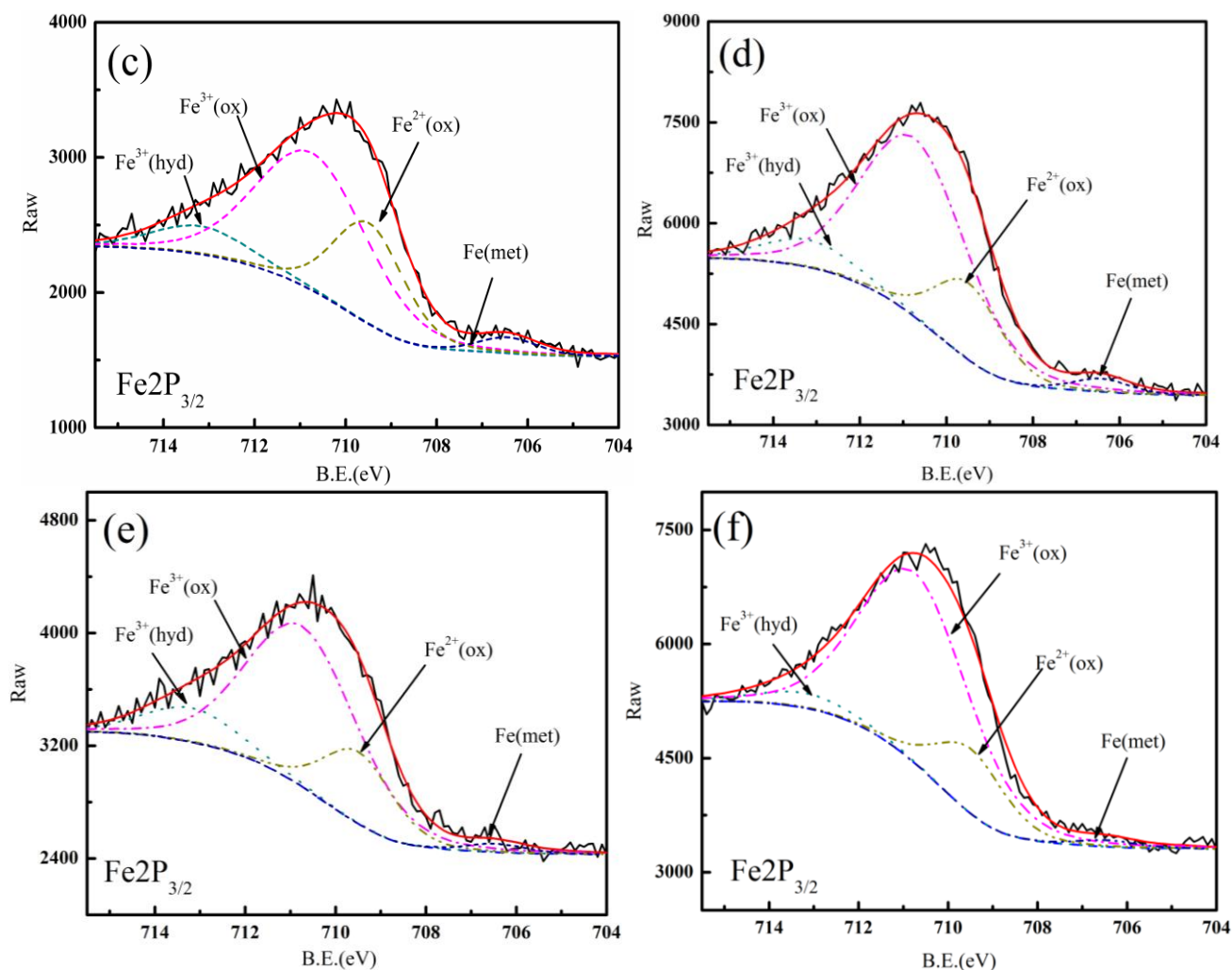


Figure 5. XPS spectra of $\text{Fe}2p_{3/2}$ in the passive film under constant stress of 100 MPa for different immersion times in 90 °C deionized water: (a) 0 day; (b) 10 day; (c) 20 day; (d) 30 day; (e) 40 day; (f) 50 day.

To obtain an in-depth understanding of the relationship between the evolution of the electrochemical properties and composition changes of the passive film, X-ray photoelectron spectroscopy (XPS) measurements were performed on different immersed samples to determine the changes in the states and contents of the various elements in the film. Fig. 5 shows the XPS results of the chemical state of Fe. The positions of the characteristic peaks apparently suggested that the film contained three compounds, FeO , Fe_2O_3 and $\text{Fe}(\text{OH})_3$.

Based on the areas of the characteristic peaks, the change in the proportion of the Fe elements in the different valence states over time was calculated, and the result is shown in Fig. 6. The Fe oxides were dominant in the initial passive film, and $\text{Fe}^{2+}(\text{ox})$, $\text{Fe}^{3+}(\text{ox})$, and $\text{Fe}^{3+}(\text{hyd})$ accounted for approximately 55%, 37%, and 8% of the total amount of the Fe element, respectively. After the immersion experiment, the proportions of $\text{Fe}^{2+}(\text{ox})$, $\text{Fe}^{3+}(\text{ox})$, and $\text{Fe}^{3+}(\text{hyd})$ changed. When the sample was immersed for 10 days, the contents of FeO and Fe_2O_3 in the film showed a significant decrease and a significant increase, respectively.

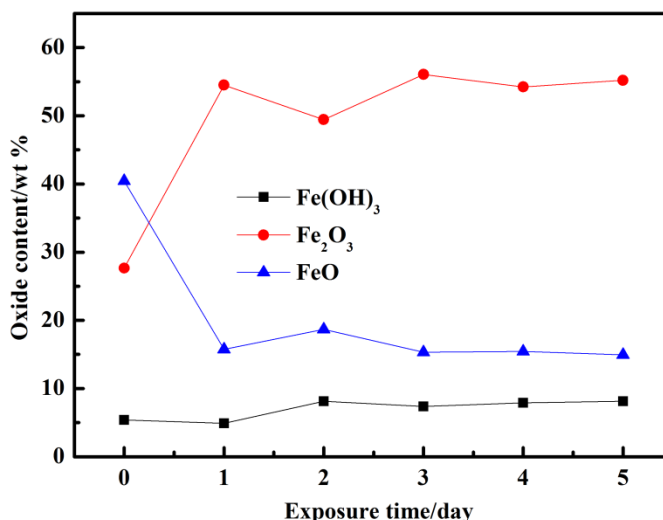
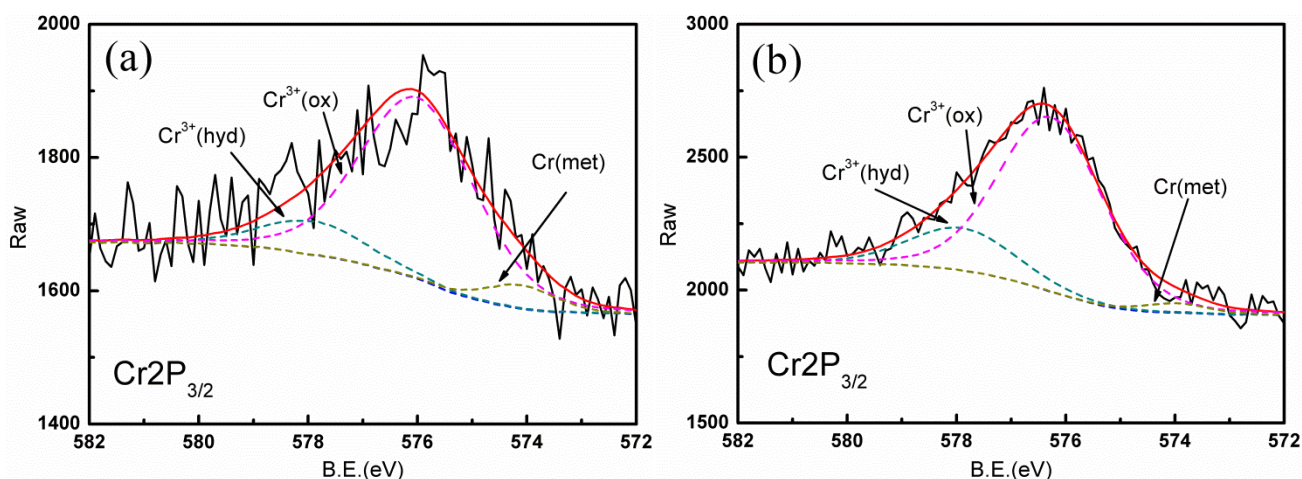


Figure 6. XPS peak area ratio of Fe_{2p_{3/2}} in the passive film under constant stress of 100 MPa for different immersion times in 90 °C deionized water.

The proportion of Fe²⁺(ox) decreased considerably from 55% to approximately 20%, while that of Fe³⁺(ox) increased from 37% to greater than 70%. When the immersion time was prolonged continuously, the contents of Fe²⁺(ox) and Fe³⁺(ox) showed a small fluctuation, and their proportions generally remained at approximately 20% and 70%, respectively. The content of Fe³⁺(hyd) exhibited a slight increase as the immersion time increased, reached a peak value of 12% after 40 days of immersion, and then fell to 5% during the prolonged immersion time.

Fig. 7 presents the XPS result of the chemical state of Cr. The characteristic peaks revealed that the film contained two compounds, Cr₂O₃ and Cr(OH)₃. The proportion of Cr³⁺(ox) and Cr³⁺(hyd) over time was calculated based on the areas of the characteristic peaks (as shown in Fig. 8). The content of Cr³⁺(ox) in the initial passive film was much higher than that of Cr³⁺(hyd), and the proportions of Cr³⁺(ox) and Cr³⁺(hyd) were 85% and 15%, respectively. During the first 20 days of immersion, the Cr³⁺(ox) content decreased remarkably, while the Cr³⁺(hyd) content increased accordingly.



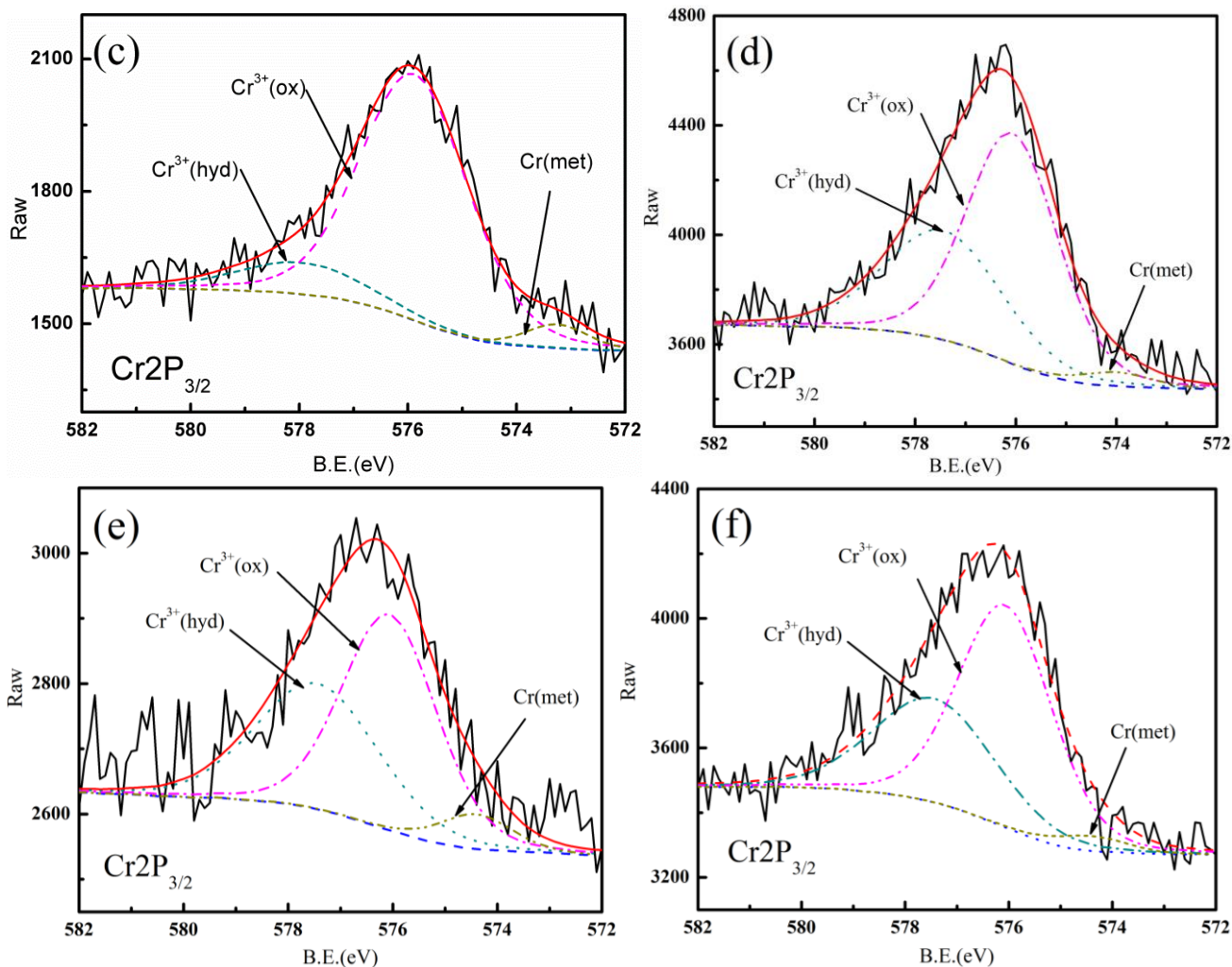


Figure 7. XPS spectra of Cr2p_{3/2} in the passive film under constant stress of 100 MPa for different immersion times in 90 °C deionized water: (a) 0 day; (b) 10 day; (c) 20 day; (d) 30 day; (e) 40 day; (f) 50 day.

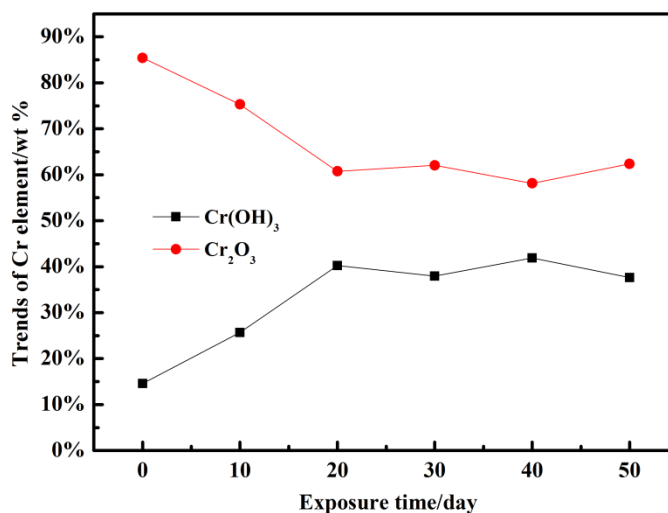


Figure 8. XPS peak area ratio of Cr2p_{3/2} in the passive film under constant stress of 100 MPa for different immersion times in 90 °C deionized water.

After 10 days of immersion, the contents of $\text{Cr}^{3+}(\text{ox})$ and $\text{Cr}^{3+}(\text{hyd})$ in the film were 75% and 25%, respectively. After 20 days of immersion, the $\text{Cr}^{3+}(\text{ox})$ content decreased to 60%, and the $\text{Cr}^{3+}(\text{hyd})$ content reached 40%. The proportions of $\text{Cr}^{3+}(\text{ox})$ and $\text{Cr}^{3+}(\text{hyd})$ generally remained unchanged when the immersion time was prolonged continuously.

To understand the changes in the contents of the different compounds in the film during immersion, the time dependence of the proportions of Cr and Fe in different valence states in the film were calculated according to the characteristic peak areas determined using XPS. As shown in the Fig. 9, the elemental oxides in the initial film accounted for approximately 90% of the total elements; among them, the contents of $\text{Fe}^{2+}(\text{ox})$, $\text{Fe}^{3+}(\text{ox})$, and $\text{Cr}^{3+}(\text{ox})$ accounted for 40%, 27%, and 23%, respectively. The hydroxides accounted for approximately 10% of the total elements; among them, the contents of $\text{Fe}^{3+}(\text{hyd})$ and $\text{Cr}^{3+}(\text{hyd})$ accounted for 6% and 4%, respectively.

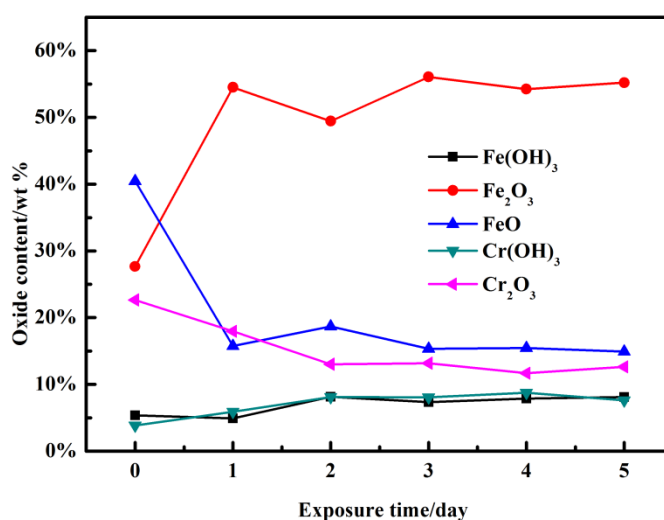


Figure 9. Changes in the proportions of compounds contained in the passive film under constant stress of 100 MPa for different immersion times in 90 °C deionized water.

After the immersion experiment, the proportion of elements in different valence states in the film changed. For the oxides, after 10 days of immersion, the FeO and Fe_2O_3 contents showed a significant decrease and increase, respectively. The proportion of $\text{Fe}^{2+}(\text{ox})$ decreased from 40% to 15%, while the proportion of $\text{Fe}^{3+}(\text{ox})$ increased from 27% to 55%. When the immersion time was further prolonged, the contents of $\text{Fe}^{2+}(\text{ox})$ and $\text{Fe}^{3+}(\text{ox})$ fluctuated slightly, and their proportions remained at approximately 15% and 55%, respectively. However, the $\text{Cr}^{3+}(\text{ox})$ content declined continuously in the early stage of immersion, and it reached and remained at 13% after 20 days. In contrast, the contents of the hydroxides exhibited a minor increase during the immersion process. The highest contents of $\text{Fe}^{3+}(\text{hyd})$ and $\text{Cr}^{3+}(\text{hyd})$ were approximately 8%.

There have been numerous studies on the formation and evolution of passive films on 304 stainless steel under different environmental conditions. The results indicated that possible Fe-containing compounds under different environmental conditions include FeO , Fe_3O_4 , Fe_2O_3 , and $\text{Fe}(\text{OH})_3$. The environmental temperature, pressure, oxygen content, and stress that the samples are subjected to have different degrees of impacts on the types and proportions of the generated

compounds [15,21,28,31]. This study found that the Fe element in the initial passive film mainly existed in the form of oxides after conventional acid cleaning and passivation, and the contents of $\text{Fe}^{2+}(\text{ox})$, $\text{Fe}^{3+}(\text{ox})$, and $\text{Fe}^{3+}(\text{hyd})$ accounted for approximately 55%, 37%, and 8% of the total amount of Fe elements, respectively. Likewise, for the same material that was tested in water environments at various temperatures, the state and content of Fe in the initially formed surface film were basically the same as the results from this paper [15,21].

After the initial passive film of the material was immersed in a high-temperature water environment for only 10 days, the $\text{Fe}^{2+}(\text{ox})$ content declined to 20%, and the $\text{Fe}^{3+}(\text{ox})$ content increased to approximately 70%. Since the increase in the Fe_2O_3 content and the decrease in the FeO content occurred at the same time, the result indicates that FeO is converted to Fe_2O_3 via further oxidation. Sun [21] reported the formation and evolution of iron-containing oxides in the film of a material after a polarization treatment in a weak acidic water environment between room temperature and 300°C , and the results were quite consistent with the results of this paper. Jung [15] showed that when the same material was exposed to a water vapor environment at 30°C , the composition of the passive film formed changed after a short period of time (1 day). The evolution of the composition was similar to that found in this study. However, when the exposure time increased to 90 days, the $\text{Fe}^{2+}(\text{ox})$ content showed an extremely slow increase or decrease. There were no significant decrease and significant increase in the $\text{Fe}^{2+}(\text{ox})$ content and $\text{Fe}^{3+}(\text{ox})$ content, respectively. The comparison of the above results suggested that a high environmental temperature and an acidic water environment can accelerate the reaction of $\text{FeO} \rightarrow \text{Fe}_2\text{O}_3$ such that most of the FeO is converted to Fe_2O_3 . However, in the neutral water vapor environments at 30 and 60°C , no sufficient chemical reaction driving force exists to form a large amount of Fe_2O_3 . In this study, the stress is apparently the main factor for the high conversion of $\text{FeO} \rightarrow \text{Fe}_2\text{O}_3$ in the initial passive film of the material. On the one hand, the relative density of FeO is 5.7, while that of Fe_2O_3 is 5.2. The formation of Fe_2O_3 can result in volumetric expansion, and tensile stress can facilitate this process. On the other hand, tensile stress can also enhance the content of adsorbed oxygen in the film and promote the complete oxidation of Fe, eventually increasing the Fe_2O_3 content. However, the proportion of Fe_2O_3 phase did not increase constantly. After 10 days of immersion, the ratio of $\text{Fe}^{2+}(\text{ox})$: $\text{Fe}^{3+}(\text{ox})$ reached 2:7 and stabilized. This finding indicates that the formation and dissolution rates of the three iron-containing compound phases in the passive film are approximately in equilibrium.

The results of this paper found that the Cr in the initial passive film mainly existed in the form of oxide Cr_2O_3 , and the proportion of $\text{Cr}^{3+}(\text{ox})$ content was 85% of the total Cr content. After the immersion experiment, the $\text{Cr}^{3+}(\text{ox})$ content decreased dramatically during the early stage of immersion, while the $\text{Cr}^{3+}(\text{hyd})$ content increased accordingly. After 20 days, the proportions of $\text{Cr}^{3+}(\text{ox})$ and $\text{Cr}^{3+}(\text{hyd})$ generally did not change. At this moment, the proportion of $\text{Cr}^{3+}(\text{ox})$ content dropped to 60%, while that of $\text{Cr}^{3+}(\text{hyd})$ content reached 40%. Related studies [21] have showed that the Cr in the passive film can exist in multiple forms such as Cr_2O_3 , CrOOH , and $\text{Cr}(\text{OH})_3$; furthermore, different Cr-containing compounds are found in different locations of the film and play different roles. $\text{Cr}(\text{OH})_3$ is first formed on the outer surface of the film during passivation, and the reaction is $\text{Cr}^{3+} + 3\text{OH}^- = \text{Cr}(\text{OH})_3$. It can be converted to Cr_2O_3 via the dehydration reaction: $\text{Cr}(\text{OH})_3 + \text{Cr} + 3\text{OH}^- = \text{Cr}_2\text{O}_3 + 3\text{H}_2\text{O} + 3\text{e}^-$. Cr_2O_3 can form a continuous dense film at the interface between

the passive film and the substrate, thus playing a role in corrosion resistance [32]. A large number of studies on the evolution pattern of Cr-containing compounds similar to those in this paper have been reported [15,21]. The environmental temperature, pH, etc. are all factors that affect the formation and evolution of Cr oxides and hydroxides.

Since the immersion experiments of all the samples in this paper were performed in a neutral water environment, stress is an important factor that affects the conversion of chromium compounds. This is because the density of $\text{Cr}(\text{OH})_3$ (3.1) is considerably lower than that of Cr_2O_3 (5.2), and the conversion of $\text{Cr}(\text{OH})_3$ to Cr_2O_3 is accompanied by strong volumetric shrinkage. Apparently, tensile stress does not favor this conversion. At the same time, the stress can also rupture the passive film, so Cr_2O_3 repeats the nucleation-rupture-nucleation process on the steel surface [35]. Due to the slow nucleation rate of Cr_2O_3 [33], the fact that the nucleation and formation of $\text{Cr}(\text{OH})_3$ occur preferentially results in a significant decrease in the ratio of $\text{Cr}^{3+}(\text{ox})/\text{Cr}^{3+}(\text{hyd})$.

XPS analysis revealed that the content of oxides in the initial passive film accounted for approximately 90% of the total elements. After the immersion experiment, the total proportion of oxides dropped slightly (85%), and the proportion of hydroxides increased to some extent. However, the relative contents of the elements in the three types of oxidized forms changed significantly within 20 days, specifically the proportion of $\text{Cr}^{3+}(\text{ox})$ decreased from 23% to 13%, which is a decrease of more than 50%. Certainly, this will adversely affect the corrosion resistance of the material. Since Cr_2O_3 has a low total content as well as a slow rate of formation and dissolution and the Fe-containing compounds exhibit high formation and dissolution rates, high temperature and high stress favor the growth of an Fe oxide layer. Therefore, an increase in the Fe oxide content of the film leads to a general decrease in the Cr_2O_3 content.

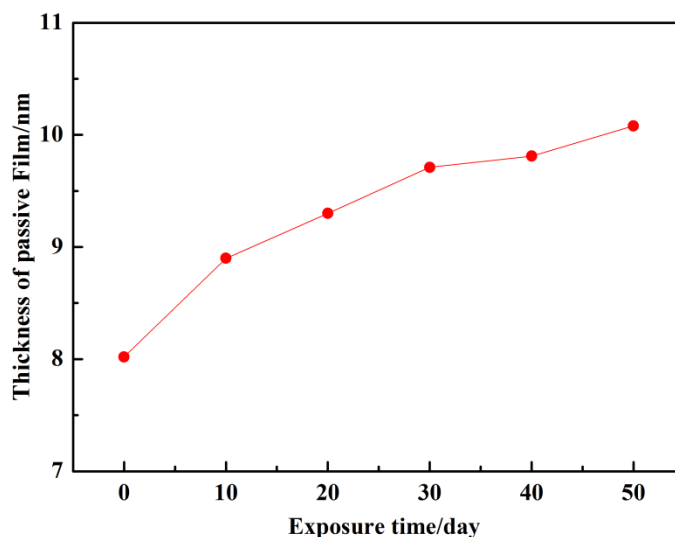


Figure 10. Variation of average thickness of the passive film with immersion times under constant stress of 100 MPa in 90 °C deionized water.

Fig. 10 shows the calculated average thickness of the passive film. The results of data analysis are shown in Table 3, and the equations are (1) and (2). As the immersion time increases, the thickness

of the film slowly increases. Researchers have reported this phenomenon [21]. This occurs because high temperatures and stresses promote film oxidation, which leads to a gradual increase in the oxide contents of the film and an increase in the average film thickness [21].

Table 3. Some of the parameters used for the calculation of average thickness of the passive film through X-ray photoelectron spectroscopy (XPS) analysis.

| Parameters | 0 Day | 10 Day | 20 Day | 30 Day | 40 Day | 50 Day |
|-------------------------------|---------|---------|---------|---------|---------|---------|
| $I_{\text{Fe}}^{\text{ment}}$ | 289.552 | 106.971 | 126.771 | 123.746 | 107.481 | 106.503 |
| $I_{\text{c}}^{\text{cont}}$ | 4790 | 10639 | 8743 | 6098 | 9350 | 6384 |
| $C_{\text{c}}^{\text{cont}}$ | 58.96 | 62.02 | 66.63 | 59.13 | 67.79 | 68.14 |
| t_{pass} (nm) | 7.94 | 8.97 | 9.16 | 9.42 | 9.56 | 10.08 |

According to the results from this paper and other studies, the compounds in the thickened part of the film were mainly Fe_2O_3 and the two hydroxides $\text{Fe}(\text{OH})^3$ and $\text{Cr}(\text{OH})_3$ [8]. Due to the low content and slow reaction rate [33], Cr_2O_3 had no apparent contribution to the film thickness.

3.3 AFM and SEM analyses

To compare the change in the surface morphology of the passive film before and after immersion in the high temperature water environment and stress conditions, AFM analysis was conducted on the samples before and after the immersion experiment. Fig. 11 presents the *three-dimensional topography AFM* images of the sample surface before immersion. As seen in Fig. 11(a), the surface of the passive film before immersion was intact, smooth and dense, and the height difference between the protruded and depressed areas was approximately 5 μm . After 10 days of immersion, the surface apparently underwent uneven corrosion, and the corrosion was mainly confined in small areas, resulting in "corrosion grooves" similar to the shape of grain boundaries. As the immersion time continuously increased, the corrosion grooves continuously increased in depth. Fig. 11(b) shows the three-dimensional morphology AFM image of the sample after 20 days of immersion, in which the depth of the corrosion grooves greatly exceeded 9 nm- the average thickness of the passive film.

Since all the studied materials had morphologies similar to that of intergranular corrosion after the immersion experiment, we removed the surface passive film by mechanical grinding and polishing to perform SEM analysis on the original substrate microstructure of the material to confirm the grain shape, size and precipitation of the second phase. Fig. 12 shows the SEM image of the metallographic structure of the material substrate. As shown in the Fig., no apparent precipitation of the second phase was found in the grain boundaries and inside the grains. The grain shape and size were highly consistent with the morphology of the areas identified as "corrosion grooves".

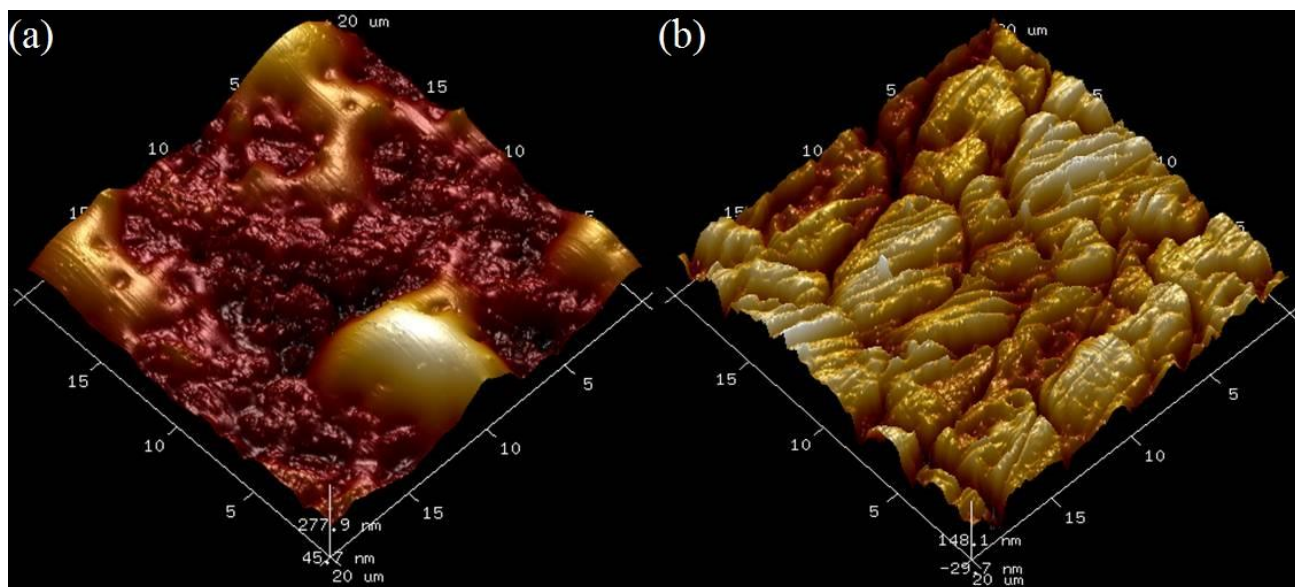


Figure 11. AFM images of the samples with passive films before and after immersion under constant stress of 100 MPa in 90 °C deionized water: (a) before immersion; (b) after 20 days of immersion.

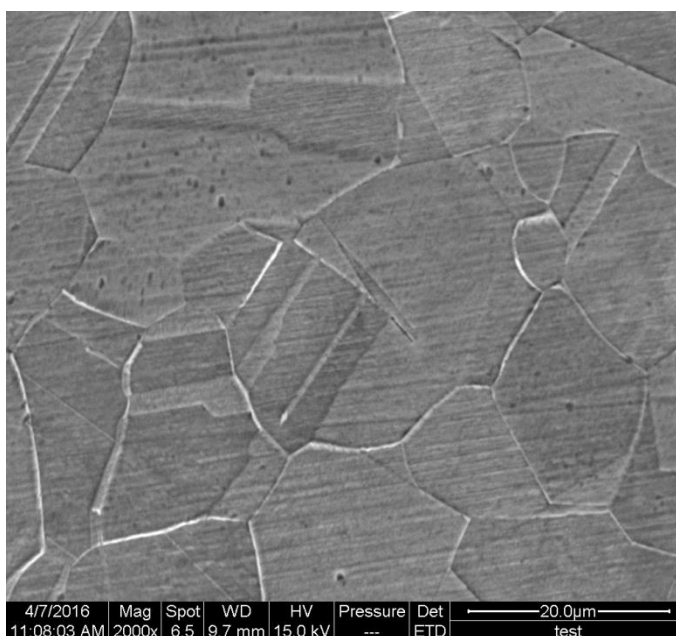


Figure 12. SEM image of the original metallographic structure of the 304 austenitic stainless steel.

The sample obtained after removing the surface passive film was immersed under the same temperature and tensile stress conditions as those in this study, and the AFM analysis was performed to examine the corrosion of the material. Fig. 13 presents the three-dimensional topography AFM image of the sample after 10 days of immersion. As seen in the Figure, the morphology surface corrosion was extremely similar to the corrosion morphology of the sample with the passive film with a grain shape consistent with the material in Fig. 12. These results demonstrate that the corrosion grooves produced

after the immersion experiment appear in the region of the austenite grain boundary of the material and are caused by intergranular corrosion.

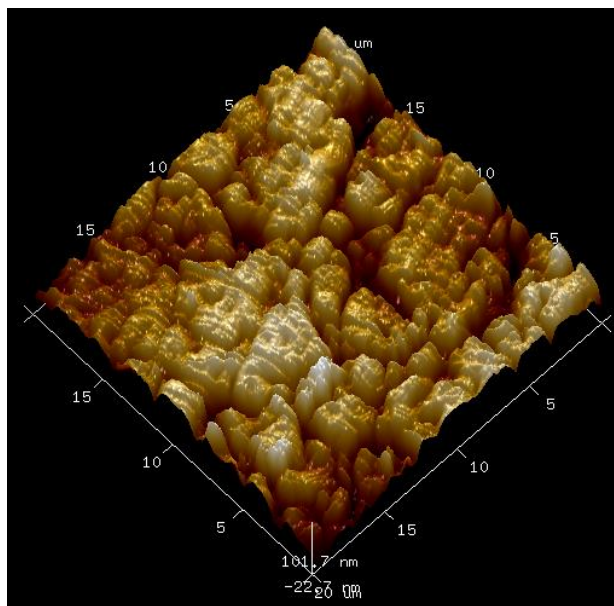


Figure 13. AFM image of sample obtained from the removal of passive film after 10 days of immersion under constant stress of 100 MPa in 90 °C deionized water.

A large number of studies [34,35] have indicated that intergranular corrosion is the most common corrosion mode for austenitic stainless steels and can cause corrosion cracking and stress corrosion cracking. The defects such as component segregation, local stress concentration and irregular arrangement of atoms exist on the substrate grain boundary. The heterogeneity of these defects is the reason for the generation of intergranular corrosion in the substrate material [36-39].

Passivation treatment can enhance the corrosion resistance of stainless steel. The main reasons for the corrosion resistance of stainless steel include the enrichment of favorable components in the passive film, the film structure being polycrystalline or amorphous, and the reduction and/or elimination of harmful impurities and defects in the film [40,41]. However, the existence of a passive film does not eliminate corrosion or intergranular corrosion of stainless steel. The reason for this property is that the heterogeneity in the microstructure, composition and structure of the surface film itself is unavoidable, which results in areas with weak corrosion resistance. Furthermore, the change in the microstructure and structure of the passive film itself during the immersion process can deteriorate the corrosion resistance. This study found that the immersion experiment caused a significant increase in the Fe_2O_3 content of the passive film, and the FeO and Cr_2O_3 contents decreased to different degrees. After 30 days of immersion, the average Fe_2O_3 content of the film increased from 28% before immersion to 55%, the average FeO content decreased from 40% before immersion to 15%, and the Cr_2O_3 content decreased from 22% before immersion to 13%. This change in composition will certainly reduce the corrosion resistance of the material.

3.4 Correlation between the evolution of the electrochemical behavior and changes in the passive films

The passive film is a "barrier" between the material substrate and the medium, and its properties directly affect the corrosion resistance of the material. The measurement results of the polarization curve demonstrated that the corrosion resistance of the material decreased as the immersion time increased, which was manifested by an apparent passivation zone in the polarization curve (0 Day) of the sample without immersion treatment. As the immersion time increased, the passivation zone of the polarization curve became narrower, and the current density increased (Fig. 2), which indicated a decrease in the corrosion resistance of the material. The same conclusion was confirmed by the electrochemical impedance spectroscopy (EIS) experiment (Fig. 4).

XPS analysis found that the oxide contents of the initial passive film of the material accounted for more than 90% of the total elements, in decreasing order of FeO, Fe₂O₃ and Cr₂O₃. During the whole immersion process, the average passive film thickness increased gradually (Fig. 10), with a total increase of 25%. The content of total oxides in the film did not considerably decrease. However, the contents of FeO and Cr₂O₃ decreased significantly in the early stage of immersion, while the content of oxide Fe₂O₃ increased significantly. The contents of FeO and Cr₂O₃ decreased by more than 60% and 55%, respectively, and the content of Fe₂O₃ increased by more than 100%.

The AES observation showed that the surface of the passive film without immersion treatment was smooth and dense (Fig. 11(a)). After the immersion experiment, intergranular corrosion occurred on the surface (Fig. 11(b)), indicating that the film was damaged. After 20 days of immersion, the depth of corrosion pits reached or exceeded the average film thickness (9 nm). At this moment, the protective effect of the passive film on the substrate disappeared essentially. This also explains the experimental results that the film resistance R_m decreased from 700 Ω to 25 Ω and then stabilized after the material was immersed for 20 days. The observation of the microstructure and the study on the characteristics of intergranular corrosion of the system demonstrate that the corrosion grooves occur in the grain boundary surface of substrate and are the result of intergranular corrosion.

As shown in this paper, the 304 stainless steel exhibited significant intergranular corrosion phenomenon after immersion in a neutral water environment at 90 °C and a stress of 100 MPa, which has not reported till now. When the surface film obtained from the conventional passivation treatment was immersed in a neutral water environment at 90 °C and below 100 MPa, its internal structure and composition first changed. In particular, the content of Cr₂O₃, which plays a major role in corrosion resistance, decreased significantly, leading to a decrease in the corrosion resistance of the passive film. The Cr₂O₃ layer that is relatively brittle under high temperature and high stress conditions could also crack [36]. The repeated nucleation-rupture-nucleation process in the solution [21] allows the dense protective layer to become porous and unstable. The dense Cr₂O₃ layer in the corroded area decreased and became porous, and the solution can even directly contact the substrate via the pores. In addition, the heterogeneities of the microstructure, composition and high stress concentration would cause intergranular corrosion and lead to the preferential dissolution and erosion of the grain boundaries. During anodic dissolution of grain boundaries, frequent ion exchange between the substrate and solution causes the corrosion grooves of the passive film to become looser, forming corrosion grooves in grain boundary region, and eventually, the protection of the passive film on substrate is lost entirely.

Cr₂O₃ enrichment can enhance the protective properties of the film [27], the defect conditions of the film and the uniformity of the surface are the primary reasons for the corrosion resistance of stainless steel [40,41]. The degree of Cr₂O₃ enrichment is a characterization of the average distribution of the compounds on the film surface and does not accurately reflect the microscopic difference of the surface. The Cr₂O₃ enrichment in the passive film with a damaged compact structure can not accurately reflect its protective properties on the substrate.

4. CONCLUSIONS

Electrochemical, XPS and AFM methods were adopted to study the evolution of the properties of a surface film formed on 304 stainless steel in a water environment at 90 °C and below 100 MPa (stress). The corrosion resistance, chemical composition and surface morphology of the film were characterized. The conclusions are as follows:

1. As the immersion time increased, the passivation zone of the polarization curve became narrower, the current density increased, and the protective properties of the film decreased.

2. After 20 days of immersion, the film resistance R_m decreased from 700 Ω to 25 Ω and stabilized. The average film thickness showed a slow increase. The content of the oxides of the initial passive film decreased from 90% to approximately 85%. Among them, the Cr³⁺(ox) content decreased from 23% to 13%, the Fe²⁺(ox) content decreased from 40% to approximately 15%, and the Fe³⁺(ox) content increased from 27% to 55%. The proportions of the Cr³⁺(hyd) and the Fe³⁺(hyd) contents slightly increased.

3. As the immersion time increased, continuous corrosion appeared on the surface along the grain boundary. The steel exhibited significant intergranular corrosion phenomenon after immersion in a neutral water environment at 90 °C and a stress of 100 MPa, which has not reported till now. The depth of the corrosion pits exceeded the average thickness of the passive film, intergranular cracks occurred on the surface film, and the protection of the passive film on the substrate was essentially lost.

References

1. V. Alar, I. Žmak, B. Runje and A. Horvatić, *Int. J. Electrochem. Sci.*, 11 (2016) 7674.
2. D.A. Fischer, L. Daille, J. Aguirre, C. Galarce, F. Armijo, R.D.L. Iglesia, G. Pizarro, I. Vargas and M. Walczak, *Int. J. Electrochem. Sci.*, 11 (2016) 6873.
3. N.A.F. Al-Rawashdeh, A.S. Alshamsi, S. Hisaindee, J. Graham and N.A. Shamisi, *Int. J. Electrochem. Sci.*, 12 (2017) 8535.
4. C.G. Tiburcio, F.H.E. López, P.Z. Robledo, J.A. Cabral, C.B. Durtewitz and F.A. Calderón, *Int. J. Electrochem. Sci.*, 11 (2016) 1080.
5. R.Y. Khaled, A.M. Abdel-Gaber and H.M. Holail, *Int. J. Electrochem. Sci.*, 11 (2016) 2790.
6. E.F. Pieretti and M.D. Neves, *Int. J. Electrochem. Sci.*, 11 (2016) 3532.
7. A. Samide, G.E. Iacobescu, B. Tutunaru and C. Tigae, *Int. J. Electrochem. Sci.*, 12 (2017) 2088.
8. M.C. Ramírez-López, L.A. Falcón-Franco, F.F. Curiel-López, P. Zambrano R, J.A. Cabral-Miramontes, C. Gaona-Tiburcio and F. Almeraya-Calderón, *Int. J. Electrochem. Sci.*, 12 (2017)

4928.

9. T. Terachi, K. Fujii and K. Arioka, *J. Nucl. Sci. Technol.*, 42 (2005) 225.
10. B.T. Lu, J.L. Luo and Y.C. Lu, *Electrochim. Acta.*, 53 (2008) 4122.
11. W.J. Kuang, X.Q. Wu, E.H. Han and J.C. Rao, *Corros. Sci.*, 53 (2011) 2582.
12. X.Q. Cheng, Z.C. Feng, C.T. Li, C.F. Dong and X.G. Li, *Electrochim. Acta.*, 56 (2011) 5860.
13. W.J. Kuang, E.H. Han, X.Q. Wu and J.C. Rao, *Corros. Sci.*, 52 (2010) 3654.
14. Y.Z. Huang and J.M. Titchmarsh, *Acta. Mater.*, 54 (2006) 635.
15. R.H. Jung, H. Tsuchiya and S. Fujimoto, *Corros. Sci.*, 58 (2012) 62.
16. Y.B. Qiu, T. Shoji and Z.P. Lu, *Corros. Sci.*, 53 (2011) 1983.
17. J.B. Huang, X.H. Liu, E.H. Han and X.Q. Wu, *Corros. Sci.*, 53 (2011) 3254.
18. C.A. Figueiredo, R.W. Bosch and M. Vankeerberghen, *Electrochim. Acta.*, 56 (2011) 7871.
19. J.B. Huang, X.Q. Wu and E.H. Han, *Corros. Sci.*, 52 (2010) 3444.
20. H. Sun, X.Q. Wu and E.H. Han, *Corros. Sci.*, 51 (2009) 2565.
21. H. Sun, X.Q. Wu, E.H. Han, *Corros. Sci.*, 51 (2009) 2840.
22. J.B. Huang, X.Q. Wu and E.H. Han, *Corros. Sci.*, 51 (2009) 2976.
23. I. Betova, M. Bojinov, P. Kinnunen, K. Lundgren and T. Saario, *Electrochim. Acta.*, 54 (2009) 1056.
24. R.W. Bosch and M. Vankeerberghen, *Electrochim. Acta.*, 52 (2007) 7538.
25. M. Bojinov, P. Kinnunen, K. Lundgren and G. Wikmark, *J. Electrochem. Soc.*, 152 (2005) B250.
26. M. Bojinov, P. Kinnunen and G. Sundholm, *Corrosion*, 59 (2003) 91-103.
27. J. Xu, X.Q. Wu and E.H. Han, *Electrochim. Acta.*, 71 (2012) 219.
28. W.J. Kuang, X.Q. Wu and E.H. Han, *Corros. Sci.*, 63 (2012) 259.
29. J.H. Ai, Y.Z. Chen, M.U. Macdonald and D.D. Macdonald, *J. Electrochem. Soc.*, 154 (2007) C43.
30. B.T. Lu, Z.K. Chen, J.L. Luo, B.M. Patchett and Z.H. Xu, *Electrochim. Acta.*, 50 (2005) 1391.
31. W.J. Kuang, X.Q. Wu and E.H. Han, *Corros. Sci.*, 52 (2010) 4081.
32. A.R. Brooks, C.R. Clayton, K. Doss and Y.C. Lu, *J. Electrochem. Soc.*, 133 (1986) 2459.
33. B.O. Elfström, *Mater. Sci. Eng.*, 42 (1980) 173.
34. J. Xu, X.Q. Wu and E.H. Han, *Electrochim. Acta.*, 71 (2012) 219.
35. Y.H. Lu, Q.J. Peng, T. Sato and T. Shoji, *J. Nucl. Mater.*, 347 (2005) 52.
36. L.J. Qiao and S.X. Mao, *Acta. Mater.*, 43 (2005) 52.
37. J.R. Galvele, *Corros. Sci.*, 36 (1994) 901.
38. R. Nishimura, I. Katim and Y. Maeda, *Corrosion*, 57 (2001) 853.
39. A.A. Elazm, R.A. Karim, I. Elmahallawi and R. Rashad, *Corros. Sci.*, 51 (2009) 203.
40. I. Betova, M. Bojinov, P. Kinnunen, K. Lundgren and T. Saario, *J. Electrochem. Soc.*, 155 (2008) C81.
41. M.F. Montemor, M.G.S. Ferreira, M. Walls, B. Rondot and M.C. Belo, *Corrosion*, 59 (2003) 11.

© 2018 The Authors. Published by ESG (www.electrochemsci.org). This article is an open access article distributed under the terms and conditions of the Creative Commons Attribution license (<http://creativecommons.org/licenses/by/4.0/>).